Ultra-clean and smoky marine boundary layers frequently occur in the same season over the southeast Atlantic

Sam Pennypacker[1], Michael Diamond[1], Robert Wood[1]

[1]Department of Atmospheric Sciences, University of Washington, Seattle, WA USA

5 *Correspondence to*: Sam Pennypacker (spenny@uw.edu)

Abstract. We study forty-one days with daily median surface accumulation mode aerosol particle concentrations below 50 cm^{-3} (ultra-clean conditions) observed at Ascension Island (7.9°S, 14.4°W) between June 2016 and October 2017 as part of the Layered Atlantic Smoke Interactions with Clouds (LASIC) campaign. Interestingly, these days occur during a period of great relevance for aerosol-cloud-radiation interactions, the southeast Atlantic (SEATL) biomass-burning season

10 (approximately June - October). That means that these critical months can feature both the highest surface aerosol numbers, from smoke intrusion into the marine boundary layer, as well as the lowest. While carbon monoxide and refractory black carbon concentrations on ultra-clean days do not approach those on days with heavy smoke, they also frequently exceed background concentrations calculated in the non-burning season from December 2016 - April 2017. This is evidence that even what become ultra-clean boundary layers can make contact with and entrain from an overlying SEATL smoke layer

15 before undergoing a process of rapid aerosol removal. Because many ultra-clean and polluted boundary layers observed at Ascension Island follow similar isobaric back-trajectories, the variability in this entrainment is likely closely tied to the variability in the overlying smoke rather than large-scale horizontal circulation through the boundary layer. Finally, surface drizzle rates, frequencies and accumulation – as well as retrievals of liquid water path – all consistently tend toward higher values on ultra-clean days. This implicates enhanced coalescence scavenging in low clouds as the key driver of ultra-clean

20 events in the southeast Atlantic marine boundary layer. These enhancements occur against and are likely mediated by the backdrop of a seasonal increase in daily mean cloud fraction and daily median liquid water path over ASI, peaking in September and October in both LASIC years. Therefore the seasonality in ultra-clean day occurrence seems directly linked to the seasonality in SEATL cloud properties. These results highlight the importance of two-way aerosol-cloud interactions in the region.

25 **1 Introduction**

Cloud-mediated aerosol radiative effects remain a significant source of uncertainty in our understanding of the climate system (Boucher et al., 2013; Rosenfeld et al., 2014). The Southeast Atlantic (SEATL) is a focal point for studying these effects because biomass-burning aerosol (BBA) particles transported from central and southern Africa frequently overly a major stratocumulus deck between approximately July and October (Devasthale and Thomas, 2011; Zuidema et al., 2016c).

The regional peak in satellite-retrieved cloud fraction and aerosol optical depth, as well as vertical overlap between the smoke layer and clouds, tends to occur between September and October (Adebiyi et al., 2015; Zuidema et al., 2016a). This establishes the potential for a complex web of aerosol-cloud-radiation interactions on seasonal and regional scales.

5   By absorbing solar radiation, BBA can alter the thermodynamic structure of the lower troposphere, leading to changes in low cloud cover (Gordon et al., 2018; Johnson et al., 2004; Sakaeda et al., 2011; Tummon et al., 2010; Yamaguchi et al., 2015; Zhou et al., 2017). If smoke entrains into the marine boundary layer (MBL) and activates into a cloud droplet, BBA may also induce indirect effects (Costantino and Bréon, 2013; Diamond et al., 2018; Zhou et al., 2017). However, contact between the base of smoke layers and the cloud-topped MBL is highly variable and difficult to constrain with satellite remote sensing
10   (e.g. (Rajapakshe et al., 2017)). At Ascension Island (ASI, details below), there is frequently heavy smoke intrusion into the MBL earlier in the burning season (June-August) than expected given the later (September-October) peak in aerosol optical depth (Zuidema et al., 2018). We should note that ASI is situated further to the west of the 'classically' defined (e.g. as by (Klein and Hartmann, 1993)) SEATL stratocumulus region. The full role of BBA in the SEATL MBL particle budget and its subsequent interactions with low clouds remains under investigation.

15

Generally, aerosol particle number concentrations in the remote MBL exhibit significant spatio-temporal variability (Allen et al., 2011; Anderson et al., 2003; Mohrmann et al., 2017). One feature of this variability observed at the surface is periods of extremely low (ultra-clean) accumulation mode (approximately 100 nm – 1 μm) number concentrations (Pennypacker and Wood, 2017; Wood et al., 2017). Wood et al. (2017) noted relative enhancements in satellite retrievals of cloud liquid water
20   path (LWP), a crucial driver of MBL coalescence scavenging (Wood, 2006), in ultra-clean air mass back trajectories several days before arriving over the Azores in the North Atlantic. Pennypacker and Wood (2017) further explored the properties of the post-frontal open cellular clouds typically associated with these ultra-clean conditions over the North Atlantic. Other studies have noted ultra-clean layers near the top of the MBL in subtropical pockets of open cells and during the stratocumulus-to-cumulus transition (Petters et al., 2006; Terai et al., 2014; Wood et al., 2018). These examples from both
25   mid-latitude and subtropical MBLs point to heavy drizzle-driven coalescence scavenging in regions of changing low cloud morphology as key for driving this particular feature of MBL aerosol variability. Drizzle also plays an important role in setting the mean MBL aerosol state under subtropical stratocumulus (Wood et al., 2012).

Our goal is to expand these analyses of ultra-clean conditions into the SEATL, especially given the potential for influence
30   from BBA. Our study is structured around the following three questions:
   1. Do ultra-clean conditions occur at the surface in the SEATL, and what is their place in aerosol variability?
   2. How do concentrations of biomass burning tracers during any ultra-clean conditions compare to background values from the non-burning season?
   3. Are ultra-clean conditions associated with enhancements in precipitation?

To address these questions, we employ observations from the first Atmospheric Radiation Measurement (ARM) Mobile Facility (AMF1) deployed to Ascension Island (7.9333°S, 14.41667°W) as part of the Layered Atlantic Smoke Interactions with Clouds (LASIC) campaign (Zuidema et al., 2016c, 2016b).

2 Data and Methods

2.1 Aerosol and Trace Gas Observations from AMF 1

A Droplet Measurement Technologies (DMT) Ultra-High Sensitivity Aerosol Spectrometer (UHSAS; Uin, 2016; DOI: 10.5439/1333828) provides aerosol number concentrations (N_A) at 0.1 Hz for particles with dry diameters between 60 nm and 1 μm. We define any day as ultra-clean if daily median N_A falls below 50 cm^{-3}. UHSAS data is currently unavailable for July 2017 due to unresolved quality control issues. Observations of total particle concentrations from a TSI Incorporated Ultrafine (>3 nm, N_{CN3}) Condensation Particle Counter (CPC) compliment the UHSAS observations (Kuang, 2016; DOI: 10.5439/1046186).

We also consider measurements of carbon monoxide (CO) and refractory black carbon (rBC) mass concentrations from AMF1. CO concentrations are measured by a Los Gatos Research trace gas analyser, while a DMT Single Particle Soot Photometer (SP2; (Sedlacek, 2017)) measures the rBC. The black carbon concentrations are calculated on 10-second intervals with a sensitivity of 10 ng m^{-3}. Our primary goal with these data (Question 2) is to determine whether ultra-clean days represent the absence of any biomass burning influence in the MBL, relative to the regional background. This background is calculated from the non-burning season between December - April. Both CO and black carbon act as biomass burning signatures, but since precipitation scavenging does not impact CO, it can reveal prior smoke contact even if aerosol concentrations are low.

2.2 Back Trajectories

Systematic differences in surface aerosol concentrations and composition at ASI, like those between ultra-clean and smoky days, could be explained by upstream differences in MBL entrainment from the free troposphere. The frequency of contact between the smoke base and MBL top over the SEATL is notoriously difficult to constrain because the aerosol often significantly attenuates lidar beams (Rajapakshe et al., 2017). Zuidema et al. (2018) also posited that changes in transport pathway from the African continent, illuminated by three-dimensional back-trajectories, were key to explaining the smokiest conditions in the MBL near ASI. We take a complimentary approach by analysing 7-day NOAA HYSPLIT isobaric boundary layer (500 m) back-trajectories initialized over ASI. For clarity, we compare the behaviour of these trajectories on ultra-clean days and days that exceed the monthly 95th percentile of daily median N_A, which we label as polluted. Isobaric

trajectories specifically reveal the origins and paths of the boundary layers that would be entraining smoke from the free troposphere.

2.3 Clouds and Precipitation

5   Based on prior analysis of ultra-clean conditions in the mid-latitude (Pennypacker and Wood, 2017; Wood et al., 2017) and subtropical (Petters et al., 2006; Wood et al., 2018) MBL, we hypothesize that enhanced drizzle also plays an important role in driving aerosol variability over the SEATL. Local surface precipitation rates at ASI are measured over a one minute averaging period using a Parsivel2 Laser Disdrometer (Delamere et al., 2016; DOI: 10.5439/1150252). We calculate a daily precipitation frequency as the ratio of these averaging periods with a detected precipitation rate to the total within a day. This

10   metric will of course not be a total drizzle frequency because it cannot include periods when precipitation evaporates before reaching the ground. We also examine differences in nonzero (i.e. only when clouds are detected) best-estimate retrievals of liquid water path from a 2-channel microwave radiometer (Cadeddu et al., 2013; Gaustad et al., 2016; DOI: 10.5439/1027369) between ultra-clean and all other days in the LASIC record. LWP is a key driver of MBL aerosol loss through coalescence scavenging even when drizzle doesn't reach the surface. In particular, we examine the statistics of

15   retrieved LWP across bins of daily median N_A (by 50 cm^{-3} from 0 - 400 cm^{-3}, by 100 cm^{-3} from 400 - 700 and then by 300 cm^{-3} from 700 - 1000 cm^{-3}). Finally, we place all of our observations in the context of the full LASIC record of both daily median MWR-retrieved LWP and cloud fraction as estimated by the ASI Total Sky Imager (Morris, 2005; DOI: 10.5439/1025308).

20 **3 Results**

3.1 Ultra-clean days

    Forty-one days meet our criteria for ultra-clean conditions (daily median $N_A <$ 50 cm^{-3}) in the available LASIC data. The 28

25   events from 2016 and the 13 events from 2017 all occur between July and November (Figure 1a). The distribution of events within these months varies, with August 2016 (12 days) and October 2017 (9 days) having the highest number of ultra-clean days in their respective years. As expected from Zuidema et al. (2018), we observe the highest daily N_A peaks in the early 2016 and 2017 biomass burning seasons (June - August). Understanding SEATL MBL aerosol variability in this crucial period thus requires an understanding of both smoke intrusions and ultra-clean conditions. In months with few or none of

30   these extremes (October 2016 - April 2017), the daily and monthly median particle concentrations vary more consistently around 200 cm^{-3}.

4

Median N_{CN3} mostly follows the same seasonal pattern as N_A across the LASIC record (Figure 1b). This leads us to expect that the accumulation mode is generally an important driver of the variability in the total particle population. On ultra-clean days, however, the accumulation is by definition mostly depleted, while daily median N_{CN3} ranges from a 115 cm^{-3} minimum to a 374 cm^{-3} maximum. The range of total particle concentrations is therefore much higher than the range within the

5   accumulation mode. On all except ultra-clean days, daily median N_A explains more than half ($r^2 = 0.65$) of the variance in the total particle concentration, as expected (Figure 1c). This relationship is substantially weaker, with the correlation statistically indistinguishable from zero ($r^2 = 0.06$), on ultra-clean days (Figure 1d). While ultra-clean days tend to have lower N_{CN3} than other days, certainly those with smoke intrusions, the weakened correlation with N_A further confirms that different processes are responsible for governing the range of total particle concentrations outside of the accumulation mode.

10   A similar difference in correlation strength between ultra-clean and other days holds at hourly time scales as well (Figure S1).

3.2 Biomass Burning Signatures

15   Perhaps unsurprisingly, CO generally tracks the accumulation mode aerosol number concentrations in Figure 1, correlating with daily median N_A most strongly ($r^2 > 0.65$) in the early biomass burning season when smoke influence in the boundary layer is highest (Figure 2a). Outside of the primary burning season, day-to-day the correlation strength varies with r^2 values between 0.04 and 0.49, depending on the month. rBC also generally follows the same patterns as aerosol number and CO (Figure 2b). The 2017 observations again confirm the analysis of Zuidema et al. (2018), which based on the 2016 data, found

20   that the signature of smoke in the ASI MBL is strongest earlier in the traditional SEATL biomass burning season. There is a smaller but noticeable peak in black carbon in January/February 2017 (Fig. 2b) that is oddly not evident in the CO observations. We leave a full diagnosis of this secondary peak for future work.

Of primary interest to this study is the range of BBA signature observations during ultra-clean events, relative to a

25   background value. Prior observations in the subtropical Southern Hemisphere have put background CO concentrations between 50 - 60 ppb (Allen et al., 2008, 2011; Shank et al., 2012). The median hourly median CO concentration on ultra-clean days is 69 ppb, with an inter-quartile range of 62 - 74 ppb, and the full distribution of ultra-clean CO concentrations exhibits some moderate bi-modality (Figure 2c). In the non-burning season (December 2016 - April 2017), the median CO concentration is 59 ppb and the inter-quartile range is between 55 and 65 ppb, consistent with the prior estimates noted

30   above. The first mode of ultra-clean CO concentrations (Fig. 2c) lines up well with these background statistics. The second mode and the tail of the distribution highlight the range of possible concentrations on ultra-clean days and pull the overall statistics toward higher concentrations relative to the background, however.

There is also certainly overlap in the ultra-clean and the non-burning background SP2 rBC (Dec. 2016, March-April 2017, Figure 2d). However, as with CO, the statistics do indicate a shift toward overall higher concentrations on ultra-clean days. Median hourly median SP2 rBC is 51 ng m^{-3} with an inter-quartile range of 23 - 120 ng m^{-3} on ultra-clean days, compared to the background median of 20 ng m^{-3} and inter-quartile range of 12 - 45 ng m^{-3}. Even the hourly extremes captured by the 5th

5 and 95th percentiles are higher on ultra-clean days (12 and 312 ng m^{-3}) than across the non-burning background (10 and 135 ng m^{-3}). In summary, there is no indication that ultra-clean days are devoid of BBA signatures or even exhibit the same distribution of smoke tracer concentrations as the non-burning season background at ASI.

Relative to the polluted extremes (recall these are defined by daily median N_A above monthly 95th percentile), there are

10 somewhat more ultra-clean 500-m isobaric back-trajectories that originate farther toward the Southern Ocean (Figure 3a). We might expect lower background aerosol concentrations and weaker influence from African biomass burning in these air masses than in those originating in the subtropics. However, there are also many polluted and ultra-clean boundary layers that follow similar isobaric trajectories on their way toward ASI (Figure 3b). In other words, the boundary layers that would be entraining free tropospheric smoke often follow very similar horizontal circulation patterns for both the highest and

15 lowest upstream extremes of N_A. This points to a key role for the variability in the horizontal and especially the vertical structure of the overlying BBA that the entraining MBL encounters.

3.3 Precipitation and Cloud Liquid Water

20 Ultra-clean days exhibit markedly different surface precipitation characteristics, as measured by the ASI Parsivel2. The distribution of precipitation rates shifts toward higher intensities on ultra-clean days (Figure 4a). Precipitation is also much more common on ultra-clean days (Figure 4b), with almost 90% of non-UC days having a precipitation frequency of less than 0.05. The tendency for more frequent and more intense precipitation inevitably leads to higher total accumulation on ultra-clean days (Figure 4c). The difference mostly stems from the shift toward more frequent drizzle conditions in ultra-

25 clean conditions. These data are all presented with cumulative distributions in order to concisely highlight the generally different behaviour of precipitation across ultra-clean days. However, the increase in drizzle intensity, frequency and accumulation also holds for ultra-clean days relative only to the distribution within their respective months (not shown).

The mean LWP retrieved by MWR measurements is higher on ultra-clean days (171 g m^{-2}) compared to other days (144 g m^{-2}

30). The standard deviations are actually larger than the mean LWP whether within ultra-clean days (182 g m^{-2}) or not (176 g m^{-2}). These statistics are further illustrated by the difference in the LWP cumulative distributions (Figure 5a). The shift is noted across most of the sampled range of LWP, though the distributions do overlap at the very highest values. While the shift toward higher LWP on ultra-clean days may not appear substantial, recall that coalescence scavenging is non-linearly

dependent on LWP (Wood, 2006). The approximately 20% increase in mean LWP on ultra-clean days would strengthen the coalescence scavenging aerosol sink by 40%.

Below a daily median N_A of about 150 cm^{-3}, daily median LWP generally increases with decreasing N_A (Figure 5b), still
5   accompanied by high variability. This is indicative of higher LWP driving reductions in accumulation mode aerosol through drizzle production and scavenging. Over a wide range of intermediate daily median N_A (~150 - 500 cm^{-3}) there is no discernible variation in binned LWP that would point to a dominant process. At higher number concentrations, however, daily median LWP continues to drop with increasing N_A, implicating at least some role for a relative lack of thick, drizzling clouds in sustaining the highest accumulation mode number concentrations.

10   **4 Discussion and Conclusions**

The SEATL remains the focus of intensive study because of the potential for direct, indirect and semi-direct radiative effects arising from extensive biomass burning aerosol layers overlying a major stratocumulus deck. We utilize data collected from an ARM Mobile Facility deployed (June 2016 - October 2017) to Ascension Island during the LASIC campaign to study 41 days with daily median accumulation mode aerosol concentrations below 50 cm^{-3}. Perhaps counter-intuitively, all of these
15   observed ultra-clean days occur between July and November, the season where BBA concentrations in the SEATL region generally peak. In the 2016 observations, ultra-clean days are particularly prevalent in July and August, and frequently both precede and follow the periods of heavy smoke intrusion into the MBL around ASI examined in Zuidema et al. (2018). In 2017, most of the ultra-clean days occur in October, but we hesitate to comment on the robustness of any interannual variability given the relatively infrequent sampling of these events and the two-year observational record. Nonetheless, both
20   years of the LASIC deployment situate ultra-clean days as a feature of surface aerosol variability at ASI during the broader SEATL biomass burning season. This naturally leads to the question of what might drive this seasonality in the occurrence of ultra-clean days.

Surface precipitation rates, frequency and accumulation, as well as retrieved cloud LWP, are all systematically enhanced on ultra-clean days relative to non-ultra clean days. These observations are indicative of vigorous coalescence scavenging being
25   a key driver of ultra-clean days at ASI. Clouds capable of initiating and sustaining this scavenging process are therefore likely precursors for these conditions. The months featuring ultra-clean days in the LASIC record are also the months leading up to and including the seasonal maximum in daily mean cloud fraction recorded by the ASI Total Sky Imager (Figure 6a). These same months also tend to be associated with the seasonal peak in daily median MWR best-estimate LWP values, though there is substantial spread in the monthly distributions in both 2016 and 2017 (Figure 6b). While limited to
30   the two-year LASIC deployment period, these local observations are broadly consistent with prior work that has noted a seasonal maximum in satellite-retrieved SEATL regional cloud fraction (Zuidema et al., 2016a) and LWP (O'Dell et al.,

2008; Zuidema et al., 2016a) between August and October. And though these satellite-based analyses tend to consider data from an area to the southeast of ASI, scavenging upwind of our observations is also likely important. Thus, the seasonality in ultra-clean day occurrence appears broadly tied to the seasonality of SEATL clouds. The increase toward the seasonal maximum in cloud cover and LWP likely provides the necessary backdrop for enhancements in coalescence scavenging

5   needed to nearly fully deplete the accumulation mode in the MBL around ASI.

However, our work further shows that using the term "ultra-clean" incompletely describes conditions with extremely low accumulation mode particle number concentrations over the SEATL. Accumulation mode and total particle concentrations are generally well correlated at ASI, though much less so on ultra-clean days, on both daily and hourly scales. Even when N_A

10   < 50 cm^{-3}, smaller particles can have $2 - 4$ times the number concentrations than in the accumulation mode. The variability of Aitken and nucleation mode particle concentrations deserves more attention in future work, including any possibility of contributions from new particle formation. Carbon monoxide and refractory black carbon mass are also not necessarily at non-burning season (December – April) background levels despite the depletion of the accumulation mode. This points to the possibility of more frequent but subtler influence of smoke in the ASI MBL outside of the most extreme intrusions like

15   those examined by Zuidema et al. (2018).

This analysis highlights an additional layer of complexity in the SEATL aerosol-cloud system. The months featuring the highest daily concentrations of aerosol particles in the MBL around Ascension Island also feature the lowest, likely due to multi-day time scale enhancements in coalescence scavenging on top of a pre-existing seasonal cycle. Ultra-clean MBL

20   conditions present an important test for large eddy simulation (LES) physics and provide a tool for further probing underlying processes and their associated timescales. The initiation, evolution and persistence of these conditions could make particularly interesting case studies for LES modelling of the Lagrangian evolution of the SEATL MBL. More broadly, air mass history is an important factor in the interpretation of aerosol-cloud interactions over the SEATL given the typical time scales associated with entrainment of free tropospheric aerosol into the MBL and loss from precipitation

25   (Diamond et al., 2018). The relative invariance of isobaric boundary layer back trajectories between ultra-clean and the most polluted days at ASI suggests that the potential for BBA entrainment set by the vertical separation of a smoke layer and the evolution of the boundary layer cloud field plays a larger role in upwind (e.g. at ASI) aerosol variability than a systematic difference in large-scale horizontal circulation in the boundary layer. The transport and consequent three dimensional structure of BBA layers certainly varies with circulation patterns above the boundary layer (Adebiyi and Zuidema, 2016).

30   The progression of clouds and precipitation along trajectories in the SEATL will depend on a number of factors, including from the influence of overlying smoke layers (Yamaguchi et al., 2015; Zhou et al., 2017). The details of how this evolution might lead to downwind ultra-clean events could be further explored in a Lagrangian LES framework. Coarser resolution models used to study aerosol-cloud interactions across the broader SEATL region should also test their capability of reproducing these events and their place in the aerosol, cloud and meteorological seasonal cycles.

Data Availability

15 All LASIC ARM data are publicly available at https://www.archive.arm.gov/discovery/. ARM dataset DOI references are included in the text.

Author Contributions

SP and RW conceived the study design and analysis. SP performed the analysis of the LASIC data. MD ran the HYSPLIT
20 transport and dispersion model to produce the back-trajectories. SP wrote the paper and all authors reviewed the manuscript.

Competing interests

The authors declare that they have no conflict of interest.

25 **Special Issue Statement**

This article is part of the special issue "New observations and related modelling studies of the aerosol–cloud–climate system in the Southeast Atlantic and southern Africa regions (ACP/AMT inter-journal SI)". It is not associated with a conference.

30

References

Adebiyi, A. A. and Zuidema, P.: The role of the southern African easterly jet in modifying the southeast Atlantic aerosol and cloud environments, Q. J. R. Meteorol. Soc., 142(697), 1574–1589, doi:10.1002/qj.2765, 2016.

5 Adebiyi, A. A., Zuidema, P. and Abel, S. J.: The convolution of dynamics and moisture with the presence of shortwave absorbing aerosols over the southeast Atlantic, J. Clim., 28(5), 1997–2024, doi:10.1175/JCLI-D-14-00352.1, 2015.

Allen, G., Vaughan, G., Bower, K. N., Williams, P. I., Crosier, J., Flynn, M., Connolly, P., Hamilton, J. F., Lee, J. D., Saxton, J. E., Watson, N. M., Gallagher, M., Coe, H., Allan, J., Choularton, T. W. and Lewis, A. C.: Aerosol and trace-gas 10 measurements in the Darwin area during the wet season, J. Geophys. Res. Atmos., 113, 1–19, doi:10.1029/2007JD008706, 2008.

Allen, G., Coe, H., Clarke, A., Bretherton, C., Wood, R., Abel, S. J., Barrett, P., Brown, P., George, R., Freitag, S., McNaughton, C., Howell, S., Shank, L., Kapustin, V., Brekhovskikh, V., Kleinman, L., Lee, Y. N., Springston, S., Toniazzo, 15 T., Krejci, R., Fochesatto, J., Shaw, G., Krecl, P., Brooks, B., McMeeking, G., Bower, K. N., Williams, P. I., Crosier, J., Crawford, I., Connolly, P., Allan, J. D., Covert, D., Bandy, A. R., Russell, L. M., Trembath, J., Bart, M., McQuaid, J. B., Wang, J. and Chand, D.: South East Pacific atmospheric composition and variability sampled along 20S during VOCALS-REx, Atmos. Chem. Phys., 11(11), 5237–5262, doi:10.5194/acp-11-5237-2011, 2011.

20 Anderson, T. L., Charlson, R. J., Winker, D. M., Ogren, J. A. and Holmén, K.: Mesoscale Variations of Tropospheric Aerosols, J. Atmos. Sci., 60(1), 119–136, doi:10.1175/1520-0469(2003)060<0119:MVOTA>2.0.CO;2, 2003.

Boucher, O., Randall, D., Artaxo, P., Bretherton, C., Feingold, G., Forster, P., Kerminen, V.-M. V.-M., Kondo, Y., Liao, H., Lohmann, U., Rasch, P., Satheesh, S. K., Sherwood, S., Stevens, B., Zhang, X. Y. and Zhan, X. Y.: Clouds and Aerosols, 25 Clim. Chang. 2013 Phys. Sci. Basis. Contrib. Work. Gr. I to Fifth Assess. Rep. Intergov. Panel Clim. Chang., 571–657, doi:10.1017/CBO9781107415324.016, 2013.

Cadeddu, M. P., Liljegren, J. C. and Turner, D. D.: The atmospheric radiation measurement (ARM) program network of microwave radiometers: Instrumentation, data, and retrievals, Atmos. Meas. Tech., 6, 2359–2372, doi:10.5194/amt-6-2359-30 2013, 2013.

Costantino, L. and Bréon, F. M.: Aerosol indirect effect on warm clouds over South-East Atlantic, from co-located MODIS and CALIPSO observations, Atmos. Chem. Phys., 13(1), 69–88, doi:10.5194/acp-13-69-2013, 2013.

35 Delamere, J., Bartholomew, M. and Shi, Y.: Laser Disdrometer (PARS2), ARM Mobile Facility (ASI) Ascension Island, South Atlantic Ocean; AMF1 (M1), Atmos. Radiat. Meas. Clim. Res. Facil. Data Arch. [online] Available from: http://dx.doi.org/10.5439/1150252, 2016.

Devasthale, A. and Thomas, M. A.: A global survey of aerosol-liquid water cloud overlap based on four years of CALIPSO-40 CALIOP data, Atmos. Chem. Phys., 11(3), 1143–1154, doi:10.5194/acp-11-1143-2011, 2011.

Diamond, M. S., Dobracki, A., Freitag, S., Griswold, J. D. S., Heikkila, A., Howell, S. G., Kacarab, M. E., Podolske, J. R., Saide, P. E., Wood, R. and Sciences, A.: Time-dependent entrainment of smoke presents an observational challenge for assessing aerosol – cloud interactions over the southeast Atlantic Ocean, Atmos. Chem. Phys., 18, 14623–14636, 45 doi:10.5194/acp-2018-461, 2018.

Gaustad, K. L., Turner, D. D. and McFarlane, S.: MWRRET Value-Added Product: The Retrieval of Liquid Water Path and Precipitable Water Vapor from Microwave Radiometer (MWR) Datasets, Washington, D.C., 2016.

50 Gordon, H., Field, P. R., Abe, S. J., Dalvi, M., Grosvenor, D. P., Hill, A. A., Johnson, B. T., Miltenberger, A. K., Yoshioka,

M. and Carslaw, K. S.: Large simulated radiative effects of smoke in the south-east Atlantic, Atmos. Chem. Phys., 18, 15261–15289, doi:10.5194/acp-18-15261-2018, 2018.

Johnson, B. T., Shine, K. P. and Forster, P. M.: The semi-direct aerosol effect: Impact of absorbing aerosols on marine
5 stratocumulus, Q. J. R. Meteorol. Soc., 130(599), 1407–1422, doi:10.1256/qj.03.61, 2004.

Klein, S. A. and Hartmann, D. L.: The seasonal cycle of low stratiform clouds, J. Clim., 6(8), 1587–1606, doi:10.1175/1520-0442(1993)006<1587:TSCOLS>2.0.CO;2, 1993.

10 Kuang, C.: Ultrafine Condensation Particle Counter Instrument Handbook, Washington, D.C., 2016.

Mohrmann, J., Wood, R., McGibbon, J., Eastman, R. and Luke, E.: Drivers of seasonal variability in marine boundary layer aerosol number concentration investigated using a steady-state approach, J. Geophys. Res. Atmos., 123, doi:10.1002/2017JD027443, 2017.

15
Morris, V. .: Total Sky Imager (TSI) Instrument Handbook, Washington, D.C., 2005.

O'Dell, C. W., Wentz, F. J. and Bennartz, R.: Cloud liquid water path from satellite-based passive microwave observations: A new climatology over the global oceans, J. Clim., 21, 1721–1739, doi:10.1175/2007JCLI1958.1, 2008.

20
Pennypacker, S. and Wood, R.: A Case Study in Low Aerosol Number Concentrations Over the Eastern North Atlantic: Implications for Pristine Conditions in the Remote Marine Boundary Layer, J. Geophys. Res. Atmos., 122, 12,393–12,415, doi:10.1002/2017JD027493, 2017.

25 Petters, M. D., Snider, J. R., Stevens, B., Vali, G., Faloona, I. and Russell, L. M.: Accumulation mode aerosol, pockets of open cells, and particle nucleation in the remote subtropical Pacific marine boundary layer, J. Geophys. Res. Atmos., 111(2), 1–15, doi:10.1029/2004JD005694, 2006.

Rajapakshe, C., Zhang, Z., Yorks, J. E., Yu, H., Tan, Q., Meyer, K., Platnick, S. and Winker, D. M.: Seasonally transported
30 aerosol layers over southeast Atlantic are closer to underlying clouds than previously reported, Geophys. Res. Lett., 44(11), 5818–5825, doi:10.1002/2017GL073559, 2017.

Rosenfeld, D., Sherwood, S., Wood, R. and Donner, L.: Climate Effects of Aerosol-Cloud Interactions, Science (80-.)., 343, 379–380, doi:10.1126/science.1247490, 2014.

35
Sakaeda, N., Wood, R. and Rasch, P. J.: Direct and semidirect aerosol effects of southern African biomass burning aerosol, J. Geophys. Res. Atmos., 116(12), 1–20, doi:10.1029/2010JD015540, 2011.

Sedlacek, A. J.: Single-Particle Soot Photometer (SP2) Instrument Handbook, Washington, D.C., 2017.
40
Shank, L. M., Howell, S., Clarke, A. D., Freitag, S., Brekhovskikh, V., Kapustin, V., McNaughton, C., Campos, T. and Wood, R.: Organic matter and non-refractory aerosol over the remote Southeast Pacific: Oceanic and combustion sources, Atmos. Chem. Phys., 12(1), 557–576, doi:10.5194/acp-12-557-2012, 2012.

45 Terai, C. R., Bretherton, C. S., Wood, R. and Painter, G.: Aircraft observations of aerosol, cloud, precipitation, and boundary layer properties in pockets of open cells over the southeast Pacific, Atmos. Chem. Phys., 14, 8071–8088, doi:10.5194/acp-14-8071-2014, 2014.

Tummon, F., Solmon, F., Liousse, C. and Tadross, M.: Simulation of the direct and semidirect aerosol effects on the
50 southern Africa regional climate during the biomass burning season, J. Geophys. Res. Atmos., 115(19), 1–20,

doi:10.1029/2009JD013738, 2010.

Uin, J.: Ultra-High-Sensitivity Aerosol Spectrometer Instrument Handbook, Washington, D.C., 2016.

5   Wood, R.: Rate of loss of cloud droplets by coalescence in warm clouds, J. Geophys. Res. Atmos., 111(21), 1–6, doi:10.1029/2006JD007553, 2006.

Wood, R., Leon, D., Lebsock, M., Snider, J. and Clarke, A. D.: Precipitation driving of droplet concentration variability in marine low clouds, J. Geophys. Res. Atmos., 117, D19210, doi:10.1029/2012JD018305, 2012.

10 Wood, R., Stemmler, J. D., Rémillard, J. and Jefferson, A.: Low CCN concentration air masses over the eastern North Atlantic: seasonality, meteorology and drivers, J. Geophys. Res. Atmos., 122, 1203–1223, doi:10.1002/2016JD025557, 2017.

15 Wood, R., O, K.-T., Bretherton, C. S., Mohrmann, J., Albrecht, B. A., Zuidema, P., Ghate, V., Schwartz, C., Eloranta, E., Glienke, S., Shaw, R. and Fugal, J.: Ultraclean layers and optically thin clouds in the stratocumulus to cumulus transition: part I. Observations, J. Atmos. Sci., 75, 1631–1652, doi:10.1175/JAS-D-17-0213.1, 2018.

Yamaguchi, T., Feingold, G., Kazil, J. and McComiskey, A.: Stratocumulus to cumulus transition in the presence of elevated
20 smoke layers, Geophys. Res. Lett., doi:10.1002/2015GL066544, 2015.

Zhou, X., Ackerman, A. S., Fridlind, A. M., Wood, R. and Kollias, P.: Impacts of solar-absorbing aerosol layers on the transition of stratocumulus to trade cumulus clouds, Atmos. Chem. Phys., 17(20), 12725–12742, doi:10.5194/acp-17-12725-2017, 2017.

25

Zuidema, P., Chang, P., Medeiros, B., Kirtman, B. P., Mechoso, R., Schneider, E. K., Toniazzo, T., Richter, I., Small, R. J., Bellomo, K., Brandt, P., De Szoeke, S., Farrar, J. T., Jung, E., Kato, S., Li, M., Patricola, C., Wang, Z., Wood, R. and Xu, Z.: Challenges and prospects for reducing coupled climate model SST biases in the eastern tropical atlantic and pacific oceans: The U.S. Clivar eastern tropical oceans synthesis working group., 2016a.

30

Zuidema, P., Alvarado, M., Chiu, C., Deszoeke, S., Fairall, C., Feingold, G., Ghan, S., Haywood, J., Kollias, P., Lewis, E., Mcfarguhar, G., Mccomiskey, A., Mechem, D., Redemann, J., Romps, D., Turner, D., Wang, H., Wood, R., Yuter, S. and Zhu, P.: Layered Atlantic Smoke Interactions with Clouds (LASIC) Science Plan, DOE/SC-ARM-14-037, , 36, 2016b.

35 Zuidema, P., Redemann, J., Haywood, J., Wood, R., Piketh, S., Hipondoka, M. and Formenti, P.: Smoke and clouds above the southeast Atlantic: Upcoming field campaigns probe absorbing aerosol's impact on climate, Bull. Am. Meteorol. Soc., 97, 1131–1135, doi:10.1175/BAMS-D-15-00082.1, 2016c.

Zuidema, P., Sedlacek III, A. J., Flynn, C., Springston, S., Delgadillo, R., Zhang, J., Aiken, A. C., Koontz, A., Muradyan,
40 P..: The Ascension Island boundary layer in the remote southeast Atlantic is often smoky, Geophys. Res. Lett., 45, 4456–4465, doi:10.1002/2017GL076926, 2018.
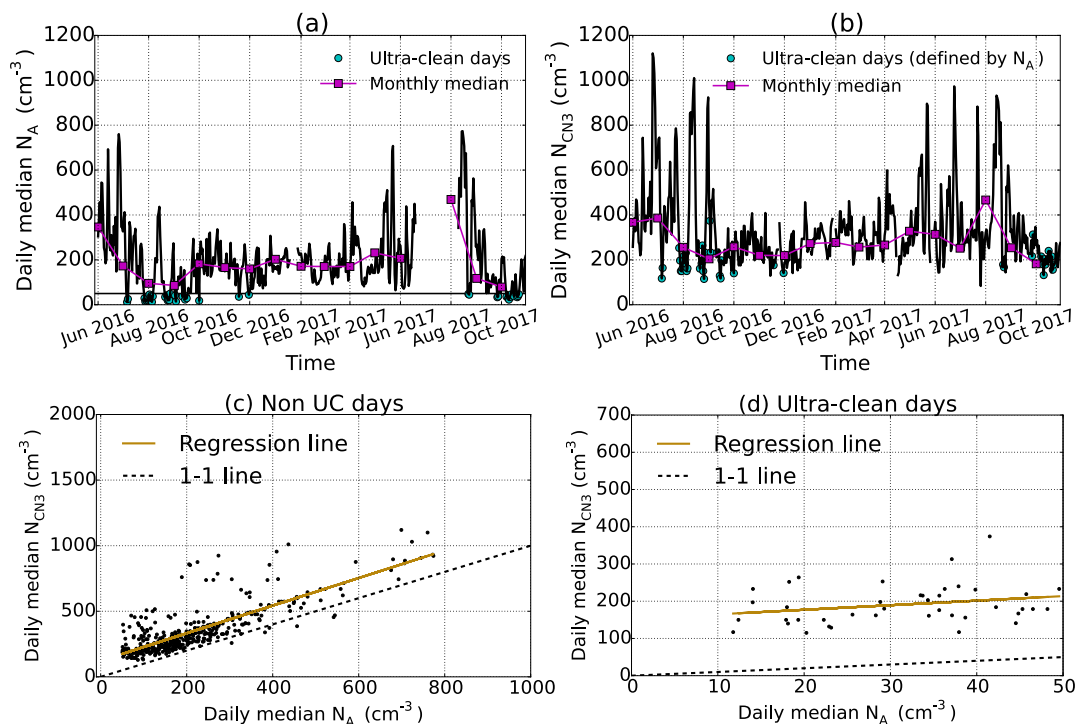
45

Figure 1: Time series of daily and monthly median (a) N_A and (b) N_{CN3} measured during LASIC, with ultra-clean days marked in cyan. Daily median N_{CN3} is then regressed against daily median N_A for both (c) non ultra-clean days and (d) ultra-clean days.
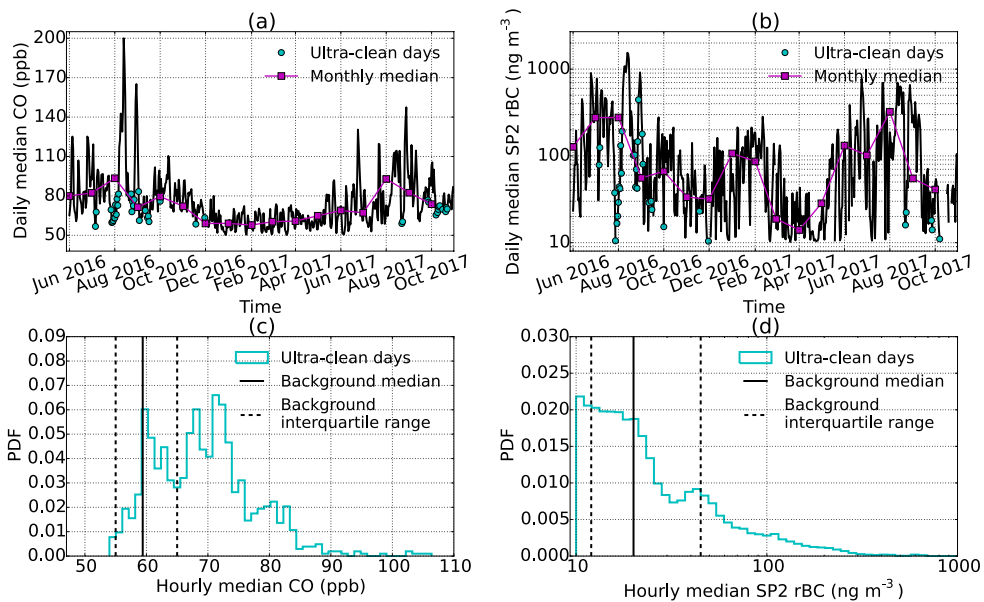
5

10

15

Figure 2: Time series of daily and monthly median (a) CO and (b) rBC measured during LASIC, with ultra-clean days marked in cyan. We then compare the PDF of hourly median (c) CO and (d) rBC from ultra-clean days to the statistics of hourly median concentrations from each tracers' respective non-burning background.
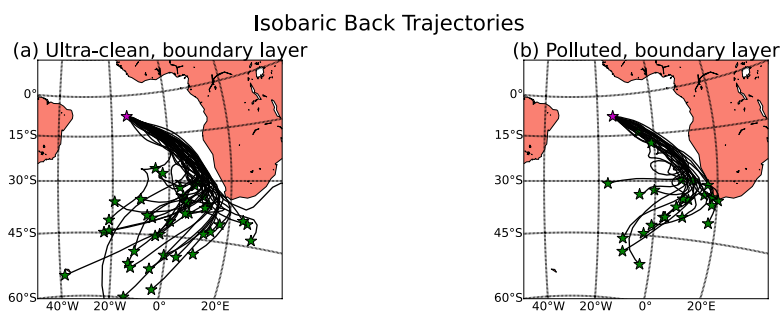
5

10

15

Isobaric Back Trajectories

Figure 3: Isobaric 7-day HYSPLIT back trajectories at 500 m for (a) ultra-clean and (b) polluted days from ASI.
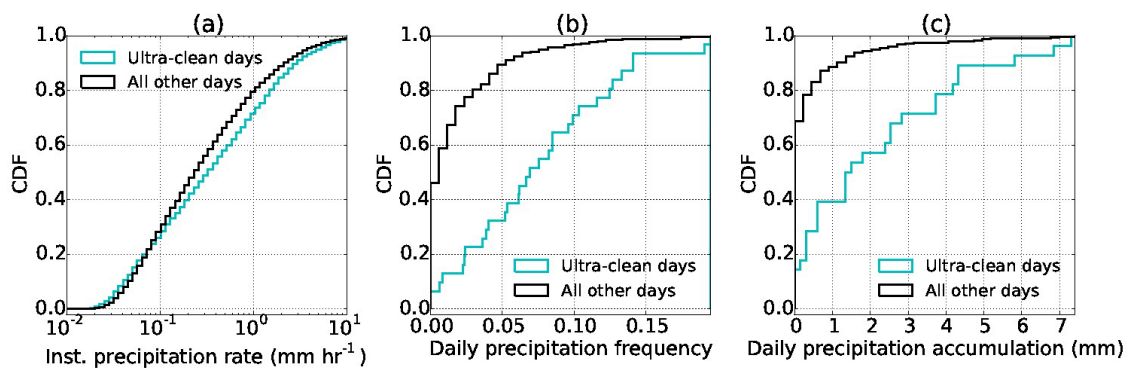
5

10

15

Figure 4: Cumulative distributions of (a) instantaneous precipitation rate, (b) daily precipitation frequency and (c) daily precipitation accumulation as measured by the ASI Parsivel2 laser disdrometer.
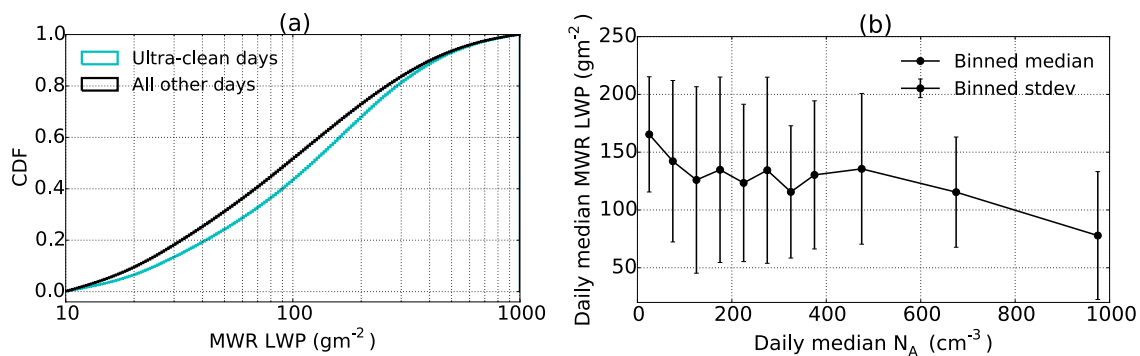
5

10

15

20

Figure 5: (a) Comparison of the cumulative distributions of best-estimate LWP retrieval from the ASI MWR between ultra-clean and all other days and (b) medians/standard deviations of daily median MWR LWP across bins of daily median accumulation mode aerosol for the entire LASIC record. In (b), bin widths were selected to account for varying density of days across the range of aerosol concentrations while still visualizing the broader pattern.
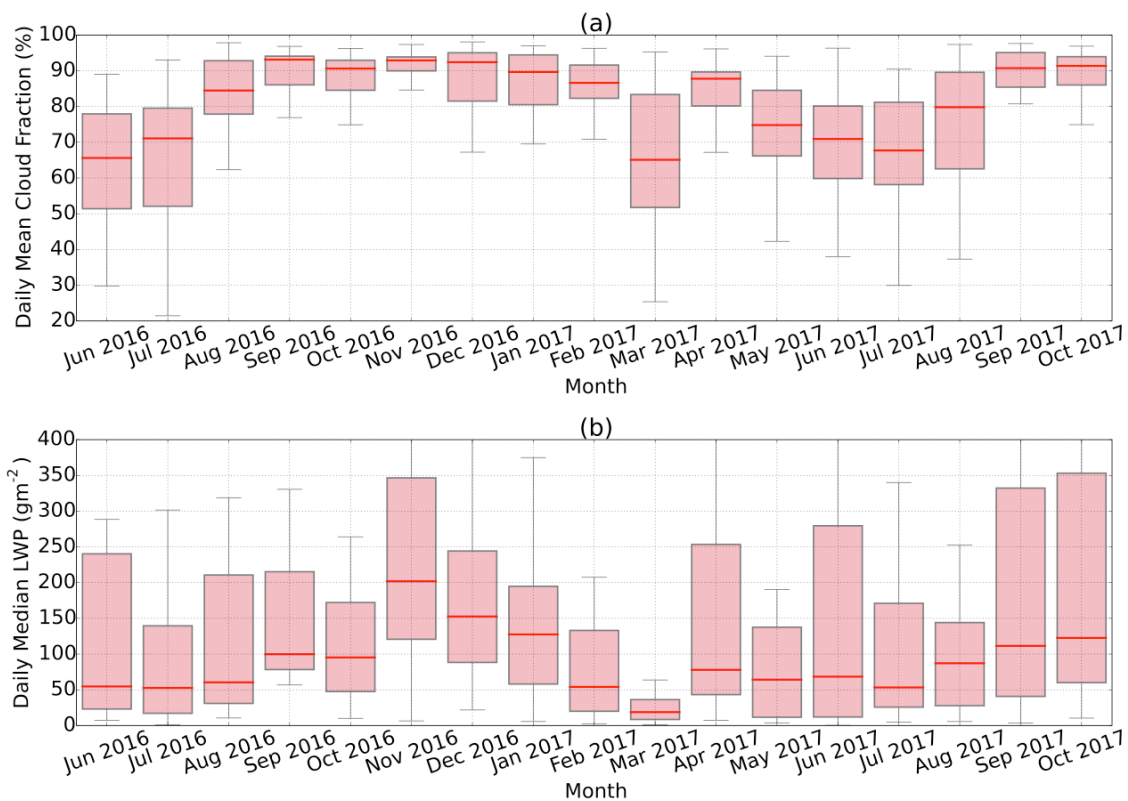
Figure 6: Monthly boxplots of (a) daily mean Total Sky Imager cloud fraction and (b) daily median MWR best-estimate LWP for each month in the LASIC record.